Precipitation of Solvent-Free $C_{60}(CO_2)_{0.95}$ from Conventional Solvents: A New Antisolvent Approach to Controlled Crystal Growth Using Supercritical Carbon Dioxide

Christian N. Field,* Paul A. Hamley, Jeremy M. Webster, Duncan H. Gregory, Jeremy J. Titman, and Martyn Poliakoff*

Contribution from the School of Chemistry, University of Nottingham, Nottingham, NG7 2RD, United Kingdom

Received June 10, 1999

Abstract: $C_{60}(CO_2)_x$, where $x = 0.2$ or 0.95, has been synthesized from solutions of C_{60} in conventional organic solvents using antisolvent precipitation with supercritical CO_2. The technique requires much lower pressures and temperatures than current routes to $C_{60}(CO_2)_x$ and, for small quantities, is quicker. Products were characterized by SEM, IR, ^{13}C solid-state NMR, and powder XRD. Reitveld refinement of the powder XRD shows CO_2 to be located in the octahedral interstitial sites of the C_{60} lattice. The cell lattice parameter is observed to increase for higher occupancies of CO_2. Experimental conditions can be varied to generate radically different morphologies of $C_{60}(CO_2)_x$. Using rapid antisolvent precipitation, irregular aggregates of ca. 200 nm particles are formed, where $x = 0.2$. With slower, diffusion-controlled precipitation, regular, highly crystalline, octahedral-shaped particles (1−70 μm) can be formed, where $x = 0.95$. All products were precipitated completely free from the original organic solvent, and we conclude that CO_2 has entered the lattice during crystallization.

Introduction

There is considerable current interest in the inclusion of gases into solid C_{60}, buckminsterfullerene. In particular, recent elegant work by the groups of Holleman[1−5] and Gadd[6,7] has shown how either CO or CO_2 can be incorporated into the C_{60} lattice at levels close to the stoichiometric 1:1 ratio of C_{60} to CO or CO_2. In these crystals, therefore, CO and CO_2 are behaving in a manner similar to conventional solvents, molecules of which cocrystallize with C_{60}. Indeed, avoiding cocrystallization of such solvents is often a difficult problem in fullerene chemistry.

The study of $C_{60}(CO_2)_x$ began with a report[8] on the effect of high-pressure CO_2 on solid C_{60} which resulted in the detectable inclusion of CO_2 in crystalline C_{60} rather than formation of $CO_2@C_{60}$. The basis of this method is that CO_2 (or another gas) is forced into solid C_{60}, and this route to $C_{60}(CO_2)_x$ has now become the method of choice[9−11] for preparing gaseous inclusion compounds of C_{60}.[12] Although the route is effective, the high pressures involved, often exceeding 150 MPa (1500 bar), have restricted this method to specialist laboratories. In this paper, we show how supercritical CO_2 ($scCO_2$) can be used to precipitate $C_{60}(CO_2)_x$ rapidly from a solution of C_{60} in conventional organic solvents. The CO_2 is incorporated as the crystallites of C_{60} are forming, and therefore, much lower pressures and temperatures are required (<100 bar, <50 °C) than in the current solid-state intercalation route[1−7] to $C_{60}(CO_2)_x$.

There has been interest in the use of supercritical fluids (SCFs) as possible solvents for C_{60} ever since its isolation as a bulk material.[13] However, neither C_{60} nor the higher fullerenes have significant solubility in common SCFs, and so these fluids have never been particularly useful in fullerene chemistry.[14] (Of course, the CO_2 used to make $C_{60}(CO_2)_x$ conventionally[6,7] is technically supercritical but the pressures are far higher than those normally used for SCF processing.)

In recent years there has been increasing research into the use of $scCO_2$ as an antisolvent for the controlled precipitation of materials from conventional solution. There is now a whole range of so-called "supercritical antisolvent" techniques for precipitation, identified by a bewildering selection of acronyms (PCA,[15−18] SEDS,[19] GAS,[20−22] SAS,[23,24] ASES,[25,26] etc.). In essence, the CO_2 is used to reduce the solvent power of a

* To whom correspondence should be addressed. http://www.nottingham.ac.uk/supercritical/.

(1) Holleman, I.; von Heldern, G.; van Bentum, P. J. M.; Engeln, R.; Nachtegaal, G. H.; Kentgens, A. P. M.; Meier, B. H.; van der Avoird, A.; Meijer, G. *Phys. Rev. Lett.* **1997**, *79*, 1138−1141.

(2) Holleman, I.; von Heldern, G.; van der Avoird, A.; Meijer, G. *Phys. Rev. Lett.* **1998**, *80*, 4899−4902.

(3) van Smaalen, S.; Dinnebier, R. E.; Schnelle, W.; Holleman, I.; von Helden, G.; Meijer, G. *Europhys. Lett.* **1998**, *43*, 302−307.

(4) van Smaalen, S.; Dinnibier, R.; Holleman, I.; von Helden, G.; Meijer, G. *Phys. Rev. B* **1998**, *57*, 6321−6324.

(5) Holleman, I.; Robyr, P.; Kentgens, A. P. M.; Meier, B. H.; Meijer, G. *J. Am. Chem. Soc.* **1999**, *121*, 199−207.

(6) Gadd, G. E.; James, M.; Moricca, S.; Cassidy, D.; Evans, P. J.; Collins, B.; Armstrong, R. S. *J. Phys. Chem. Solids* **1998**, *59*, 1383−1391.

(7) James, M.; Kennedy, S. J.; Elcombe, M. M.; Gadd, G. E. *Phys. Rev. B* **1998**, *58*, 14780−14785.

(8) Nagano, Y.; Kiyobayashi, T.; Nitta, T. *Chem. Phys. Lett.* **1994**, *217*, 186−190.

(9) Gadd, G. E.; Moricca, S.; Kennedy, S. J.; Elcombe, M. M.; Evans, P. J.; Blackford, M.; Cassidy, D.; Howard, C. J.; Prasad, P.; Hanna, J. V.; Burchwood, A.; Levy, D. *J. Phys. Chem. Solids* **1997**, *58*, 1823−1832.

(10) Morosin, B.; Jorgensen, J. D.; Short, S.; Kwei, G. H.; Schirber, J. E. *Phys. Rev. B* **1996**, *53*, 1675−1678.

(11) Morosin, B.; Assink, R. A.; Dunn, R. G.; Massis, T. M.; Schirber, J. E.; Kwei, G. H. *Phys. Rev. B* **1997**, *56*, 13611−13614.

(12) Indeed, $C_{60}(CO_2)_x$ may have inadvertently been made earlier by Johnson et al., who briefly describe using $scCO_2$ in their sample preparation (Johnson, R. D.; Yannoni, C. S.; Dorn, H. C.; Salem, J. R.; Bethune, D. S. *Science* **1992**, *255*, 1235−1238).

(13) Kratchmer, W.; Lamb, L. D.; Fostiropoulos, K.; Huffman, D. R. *Nature* **1990**, *347*, 354−358.

(14) Siam, S.; Kuo, K. C.; Stalling, D. L. *Sep. Sci. Technol.* **1993**, *28*, 1509−1525.

(15) Dixon, D. J.; Johnston, K. P. *J. Appl. Polym. Sci.* **1993**, *50*, 1929.

10.1021/ja9919478 CCC: $19.00
Published on Web 03/04/2000

conventional solvent so that the solute precipitates. The pressure, temperature, and flow rates of the $scCO_2$ are manipulated to achieve the desired particle size, shape, and morphology of the precipitated material.

C_{60} particles have potential medicinal applications in areas such as genetic transcription and neuroprotection, showing an ability to cleave DNA and to scavenge radicals.[27] These applications require the fullerenes to be in an aqueous medium. To overcome the inherent hydrophobicity of fullerenes, several approaches have been tried: encapsulation, functionalization, and suspension. To create a suspension of C_{60} in water, there is a need for efficient ways of producing C_{60} with a very small particle size. Here we demonstrate a new way of producing C_{60} as a solvent-free yellow powder with a particle size of ca. 200 nm.

In this paper, we describe the formation of $C_{60}(CO_2)_x$ powders and microcrystals by supercritical antisolvent precipitation from solutions of C_{60} in toluene and 1,2-dichlorobenzene. Scanning electron microscopy (SEM) shows that diverse particle sizes and morphologies can be prepared in a controlled manner using this precipitation technique. What is particularly interesting is that the crystals of $C_{60}(CO_2)_x$ precipitated in this way are apparently free from detectable amounts of the organic solvent; CO_2 appears to be incorporated preferentially into the C_{60} lattice. The presence of included CO_2 and the complete absence of included organic solvents is most clearly demonstrated in the IR spectra. Solid-state ^{13}C NMR MAS spectra reveal a maximum CO_2:C_{60} ratio of 1:63, corresponding to $C_{60}(CO_2)_{0.96}$, and suggest that the presence of CO_2 hinders the rotation of the C_{60} molecules on their lattice site. The powder X-ray diffraction pattern is consistent with previously published work[6] and thus conclusively identifies the product as $C_{60}(CO_2)_x$. The lattice parameter, calculated from the XRD data, shows an increase with increasing CO_2 occupancy. Reitveld refinement on the powder XRD of the product confirms that CO_2 resides in the octahedral interstitial sites of the C_{60} lattice, and the amount of CO_2 is deduced in the refinement, giving the product as $C_{60}(CO_2)_{0.94}$.

Experimental Section

C_{60}, buckminsterfullerene, was received as a black crystalline powder (origin MTR Ltd., Cleveland, OH), and its purity was checked by IR microscopy and ^{13}C solid-state NMR. Traces of cyclohexane were observed by IR and ^1H solution NMR in both the starting material, C_{60}, and the toluene (Analar or Technical grades) and in some of our products.

C_{60} was dissolved in toluene (2.8 mg mL^{-1}) or 1,2-dichlorobenzene (27 mg mL^{-1}) to give a characteristic purple solution which was filtered prior to use. The antisolvent, CO_2, was of a 99.95% purity grade as used in the food industry. See Figures 1−3 for diagrams of the apparatus used.

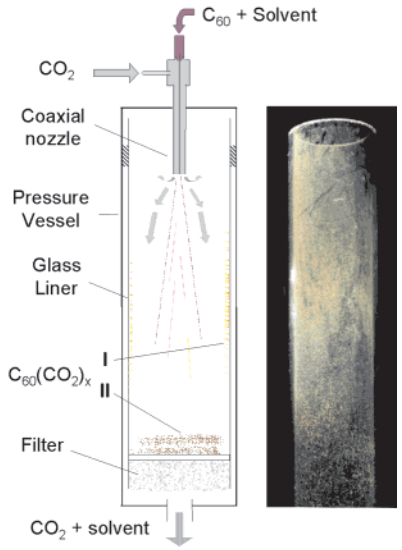

Figure 1. PCA precipitation method. CO_2 and the toluene solution meet at the exit of the coaxial nozzle. A photograph of the yellow product **I** formed on the walls of the glass liner from the pressure vessel is shown alongside the schematic description of the equipment.

In the PCA precipitation method, the C_{60} solution was injected into a flow (30 mL min^{-1} of liquid CO_2) of near-critical (25−31 °C, >73.8 bar) or supercritical (>31 °C, >73.8 bar) CO_2. The resultant precipitate consisted of a very fine layer of mustard-yellow colored particles, **I**, on the walls of the glass liner (Figure 1) and of a much thicker dark brown layer, **II**, packed farther downstream onto the filter paper and glass wool. The ratio of yellow **I**:brown **II** product was increased by using higher CO_2 flow rates and increased temperatures, in line with increased turbulence and more rapid mixing with the organic solvent. The fine powder, **I**, was particularly difficult to handle. When scraped with a spatula, it immediately aggregated into a dark brown solid, similar to **II**. The PCA experiments typically produced ca. 20 mg of material, sufficient for analysis by FT-IR microscopy, SEM, powder XRD, and, by combining material from identical experiments, ^{13}C solid-state NMR. With reference to Figure 1, CO_2 and the toluene meet at the end of the coaxial nozzle. This nozzle is similar to that built by Johnston and co-workers[28] using stainless steel pipe, $^1/_{16}$-in. o.d. and 800 μm i.d., to carry the CO_2, inside which is a capillary carrying the organic solution, 75 or 220 μm i.d. The CO_2 flow rate was set at 30 mL min^{-1} of liquid CO_2 (the pneumatic pump used (NWA PM101) condenses CO_2 at around 5 °C from the cylinder at approximately 50 bar, giving a CO_2 density of 0.9 g mL^{-1}, at 30 mL min^{-1} = 27 g min^{-1}). The organic solution (2.8 mg mL^{-1} C_{60} in toluene) was injected at a rate of 0.33 mL min^{-1}. Neat solvent was pumped through the capillary for 15 min prior to precipitation to ensure steady-state conditions in the vessel (≈1% toluene in CO_2). The critical temperature and pressure of the CO_2−1% toluene solvent system have been calculated[29−32] (T_c = 37.2 °C, P_c = 79.3 bar) and are exceeded during the experiment, ensuring supercritical conditions throughout the precipitation. A lower temperature, as used in earlier experiments, results in a homogeneous CO_2−toluene liquid phase, yielding identical products. The steel pressure vessel has a volume of ≈30 mL. It is lined with a thin glass

(16) Mawson, S.; Yates, M. Z.; O'Neill, M. L.; Johnston, K. P. *Langmuir* **1997**, *13*, 1519.
(17) Mawson, S.; Johnston, K. P.; Betts, D. E.; McClain, J. B.; DeSimone, J. M. *Macromolecules* **1997**, *30*, 71.
(18) Mawson, S.; Kanakia, S.; Johnston, K. P. *Polymer* **1997**, *38*, 2957.
(19) Palakodaty, S.; York, P.; Hana, M.; Pritchard, J. *Proc. 5th Meeting on Supercritical Fluids, Nice, France* **1998**, *T1*, 275.
(20) Gallagher, P. M.; Coffey, M. P.; Krukonis, V. J.; Hillstrom, W. W. *J. Supercrit. Fluids* **1992**, *5*, 130.
(21) Yeo, S.-D.; Lim, G.-B.; Debendetti, P. G.; Bernstein, H. *Biotechnol. Bioeng.* **1992**, *41*, 341.
(22) Randolph, T. W.; Randolph, A. D.; Mebes, M.; Yeung, S. *Biotechnol. Prog.* **1993**, *9*, 429.
(23) Reverchon, E.; Porta, G. D.; Trolio, A. D. *Proc. 4th Conf. on Supercritical Fluids and Their Applications, Capri, Italy* **1997**, 335.
(24) Reverchon, E.; Barba, A. A.; Porta, G. D.; Ciambelli, P.; Sannino, D. *Proc. 4th Conf. on Supercritical Fluids and Their Applications, Capri, Italy* **1997**, 385.
(25) Bleich, J.; Müller, B. W.; Wassmus, W. *Int. J. Pharm.* **1993**, *97*, 111.
(26) Bleich, J.; Müller, B. W. *Microencapsulation* **1996**, *13*, 131.
(27) Da Ros, T.; Prato, M. *Chem. Commun.* **1999**, 663−669.
(28) Mawson, S.; Kanakia, S.; Johnston, K. P. *J. Appl. Polym. Sci.* **1997**, *64*, 2105−2118.
(29) Calculations were performed for critical points of the CO_2−toluene mixture described by the Peng−Robinson[30] equation of state. Mixture parameters were obtained by fitting experimental data from the literature,[31] and a computational algorithm developed by Heidemann and Khalil[32] was employed to obtain values of T_c and P_c at a given mixture composition.
(30) Peng, D. Y.; Robinson, D. B. *Ind. Eng. Chem. Fundam.* **1976**, *15*, 59.
(31) Ng, H.-J.; Robinson, D. B. *J. Chem. Eng. Data* **1978**, *23*, 325.
(32) Heidemann, R. A.; Khalil, A. M. *AIChE J.* **1980**, *26*, 769.

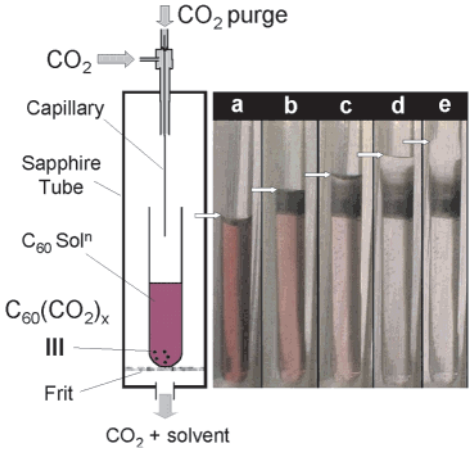

Figure 2. (Left) Apparatus initially used for controlled crystallization using a compressed antisolvent with precipitation here on a small scale, <5 mg per run, allowing for IR and SEM characterization. (Right) Series of photographs of C_{60}−toluene solution, contained in a quartz tube and held within the sapphire pressure vessel, recorded at 45 °C in situ during a precipitation experiment with CO_2. The arrows indicate the position of the meniscus as the pressure of CO_2 is increased. (a) 1 bar, purple C_{60} toluene solution with well-defined meniscus; (b) 46 bar, the solvent level has risen as indicated, precipitation on the walls of the tube has occurred in this expanded solvent region, and the bulk solution is paler; (c) 53 bar, solvent level continues to rise, precipitation begins in the bulk solution which is now only lightly colored; (d) 75 bar, meniscus starting to blur, precipitate collects in bottom of tube; (e) 83 bar, toluene phase colorless, meniscus blurred as CO_2 and toluene diffuse into each other. At 83 bar nearly all the C_{60} had precipitated and the solvent was removed using a CO_2 flow.

tube of inner diameter 11.9 mm, fitted tightly in place to ensure gas flow through the tube. A set of filter papers backed by a glass wool plug is placed at the exit of the tube to contain the precipitate. The glass liner can be removed, and samples can be kept intact for future reference. The pressure vessel was housed in an oven maintained at a steady temperature in the range 25−45 °C. A length of coiled stainless steel pipe carrying the CO_2 is also housed in the oven and ensures efficient preheating of the CO_2.

Figure 2 illustrates the apparatus used for controlled crystallization, using a compressed antisolvent with precipitation on a small scale, <5 mg per run, allowing for FT-IR and SEM characterization. The antisolvent, CO_2, is pressurized and injected using a cooled HPLC pump (Gilson 303). A sapphire tube of inner diameter 7.8 mm (volume 6 mL) replaces the steel pressure vessel used in the PCA experiments and is similarly housed in an oven. These experiments were carried out at both 45 and 60 °C. A shortened 5-mm quartz NMR tube, of inner diameter 4.2 mm, is placed inside the sapphire tube and contains ca. 0.5 mL of an organic solution, e.g. a saturated solution of C_{60} in toluene (2.8 mg mL^{-1}) or 1,2-dichlorobenzene (27 mg mL^{-1}). The mass fraction of CO_2 in toluene varies throughout the experiment. The CO_2 is injected in exactly the same way as for the traditional PCA experiment shown in Figure 1. The most efficient way to remove the toluene after precipitation was by the rapid injection of CO_2 down a capillary positioned at the open end of the quartz tube.[33] The turbulence of this CO_2 stream caused rapid mixing and allowed subsequent removal of the solvent. On-line IR spectroscopy is used to monitor the level of solvent in the CO_2 leaving the vessel. This experiment was also repeated using a solution of C_{60} in 1,2-dichlorobenzene. On occasion, it was not always possible to remove all of the solvent using $scCO_2$, and in these cases the CO_2 could be observed outgassing from the residual solvent during depressurization with interesting effects on the precipitated material. The SEM results showed an interesting morphology, see Figure 4d,f.

(33) An alternative approach for removing the solvent was tried unsuccessfully where the CO_2 density was greatly increased, by raising the system pressure, in an attempt to make the CO_2 phase more dense than that of the solvent and so "float" the solvent away.

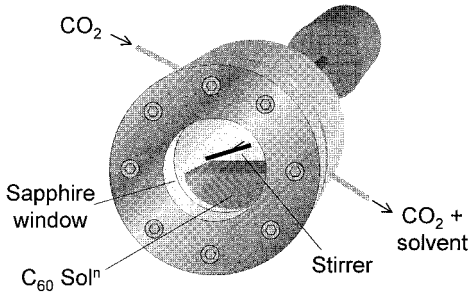

Figure 3. Diagram of the large-volume view cell which was used to prepare these crystalline products, $C_{60}(CO_2)_{0.95}$, on a larger scale, >100 mg per run, for IR, SEM, XRD, and ^{13}C NMR.

Figure 3 shows a diagram of the pressure vessel used for scale-up of the controlled crystallization experiment shown in Figure 2. The precipitation vessel (NWA GmbH, Lörrach, Germany) was a high-pressure view cell consisting of a steel barrel, inner diameter 36 mm and internal volume ≈20 mL, with a stirrer at one end to allow gentle mixing of the solvent with the antisolvent after precipitation had taken place. The other end of the steel barrel was closed with a 3 cm-thick sapphire window through which the crystallization process could be observed. Five milliliters of a saturated organic solution of C_{60} in 1,2-dichlorobenzene (27 mg ml^{-1}) was carried in a glass boat, capacity 6 mL, which was placed inside the cell prior to pressurization. The cell temperature was maintained at 45 °C by cartridge heaters inserted into the cell body, and the temperature inside the cell was measured directly by a separate thermocouple. The CO_2 plumbing to and from this larger volume view cell was essentially the same as that described above for the apparatus shown in Figure 2.

Scanning electron micrographs (SEM) were measured on a JEOL WinSEM 6400 microscope. The products were mounted on an adhesive carbon layer stuck onto an aluminum stub and sputtered with a thin layer of gold.

IR spectra were recorded on precipitated material without any sample preparation using a Perkin-Elmer Model i-Series IR microscope with a liquid nitrogen-cooled, narrow-band MCT detector attached to a PE System 2000 interferometer using a resolution of 4 cm^{-1}.

Carbon-13 solid-state magic angle spinning (MAS) NMR spectra were recorded at 293 K at a resonance frequency of 75.46 MHz. A 7.5-mm double-resonance MAS probe was used to acquire data of both the starting material and products **II** and **III** at spinning rates of 1 and 4 kHz, regulated to within ±2 Hz. Experimental parameters were as follows: relaxation delay, 60 s; acquisition time, 68 ms; carbon-13 $\pi/2$ pulse length, 4 μs; spectral width, 30 kHz. Between 512 and 1024 scans were acquired for each spectrum, and exponential line broadening of 40 Hz was applied prior to Fourier transformation of the FID.

Powder X-ray diffraction studies were undertaken using a Philips XPERT Θ−2Θ diffractometer using a Cu Kα radiation source. Indexing was performed on diffraction data from samples run between $5° \le 2\theta \le 80°$, over scan durations of 16 h. XRD patterns were indexed using DICVOL91[34,35] and refined by least-squares fitting. Diffraction data suitable for structure refinement were collected over a duration of 16 h in the range 5−80° 2θ with step size 0.02° 2θ at 298 K. Full profile Rietveld refinement[36] was performed on the product **III**, using the Philips PC Rietveld Plus package[37,38] with refined lattice parameters obtained from indexing and fitting.

Safety Note: These experiments involve high pressures and should be approached with caution.

Results and Discussion

The crystallites described in this paper were prepared using the two different precipitation strategies outlined in Figures 1−3. The strategies differ in the speed with which precipitation occurs

(34) Louer, D.; Louer, M. *J. Appl. Crystallogr.* **1972**, *5*, 271.
(35) Boultif, A.; Louer, D. *J. Appl. Crystallogr.* **1991**, *24*, 987.
(36) Reitveld, H. M. *J. Appl. Crystallogr.* **1969**, *2*, 65.
(37) Wiles, D. B.; Young, R. A. *J. Appl. Crystallogr.* **1981**, *14*, 149.
(38) Howard, C. J.; Hill, R. *J. A. A. E. C. Rep.* **1986**, No. M112.

and hence in the size and composition of the precipitated crystallites. The first strategy involves precipitation with a compressed antisolvent (PCA)[15−18] (Figure 1), where the C_{60} is dissolved in an organic solution and pumped through a narrow capillary into a concurrently flowing antisolvent, supercritical or liquid CO_2; for a more detailed description, see the Experimental Section above. The CO_2 very rapidly reduces the solvent power of the organic solvent due to efficient mixing of solvent and antisolvent, causing the C_{60} to precipitate. The design of the nozzle facilitates atomization of the C_{60} solution as it exits the capillary, producing very small droplets of C_{60} solution. Diffusion of CO_2 into these tiny solvent domains is aided by the low viscosity of $scCO_2$, resulting in submicron C_{60} particles. The turbulence of the CO_2 stream enables the C_{60} to be dried rapidly, thus inhibiting aggregation. An unusual feature of our equipment is the glass liner, placed inside the pressure vessel,[39] on which the product is precipitated. In this way the product can be removed without disturbance for inspection (see Figure 1).

The second precipitation strategy is a new extension of the GAS technique.[20−22] In our approach, the CO_2 antisolvent is added slowly to the pressure vessel, and mixing of the antisolvent with the solution relies entirely on diffusion between the two layered phases (see Figure 2). Thus, the solvent power of the organic solvent is reduced very slowly as the amount of CO_2 dissolved in the solution is increased; crystallization starts at fewer nucleation sites, and slow growth of larger crystallites is encouraged. As the pressure, and hence the mole fraction, of CO_2 increases, the system changes from two phases at lower pressures (see Figure 2a−d) to one phase at high pressure (see Figure 2e), where the pressure is greater than 80 bar and mole fraction is greater than 0.86. These observations have been supported by preliminary calculations[31,40] using the Peng−Robinson[30] equation of state to model the CO_2−toluene phase behavior. Figure 2 also shows how "slow" precipitation of $C_{60}(CO_2)_x$ proceeds from toluene solution, at 45 °C, as the pressure of CO_2 is increased (ca. 1 bar min^{-1}). By 50 bar, the toluene solution was almost colorless and the C_{60} had precipitated as a black product, **III**, at the bottom of the tube. After precipitation was complete, the cell was purged with CO_2 to remove the solvent. Two solvents were used, toluene as discussed above ($\rho = 0.87$ g cm^{-3}, bp = 111 °C) and 1,2-dichlorobenzene ($\rho = 1.31$ g cm^{-3}, bp = 180 °C). Their behavior with the antisolvent CO_2 was quite different. Toluene has a density closer to that of supercritical CO_2 ($\rho_c = 0.47$ g cm^{-3}) and so mixes more easily, creating a deep CO_2−toluene phase during the experiment (see Figure 2) and allowing relatively quick removal of the organic solvent after precipitation. 1,2-Dichlorobenzene is a better solvent for C_{60} but, with its higher density and boiling point, did not mix as efficiently with the CO_2 phase, and a narrow CO_2−1,2-dichlorobenzene phase was observed above the organic solution. In toluene, the precipitation of $C_{60}(CO_2)_x$ occurs at subcritical pressures due to the high solubility of CO_2 in toluene. When 1,2-dichlorobenzene is used, higher pressures are needed to aid mixing. Nevertheless, it was possible to grow highly crystalline samples of $C_{60}(CO_2)_x$ from both solvents. We found that the onset of precipitation appeared to be dependent upon the rate of CO_2 pressurization, "rapid" pressurization (ca. 8 bar min^{-1}) resulting in the onset of particle formation at a higher pressure. This may be due to the kinetics of CO_2 dissolution in the toluene, slower pressurization (ca. 1 bar min^{-1}) allowing the amount of CO_2 dissolved in the toluene to reach equilibrium. It is the concentration of CO_2 in the organic phase which we believe triggers precipitation in these experiments. In addition, the surface area of the C_{60} solution exposed to the CO_2 will also affect the kinetics of CO_2 mixing, likewise the geometry of the vessel used to contain the C_{60} solution. However, no detailed study of these parameters was attempted as the desired chemical nature of the product appears to be independent of these factors.

A second pressure vessel was assembled to allow "slow" crystallization on a much larger scale (>100 mg). A diagram of the apparatus is shown in Figure 3, and the apparatus is described in more detail in the Experimental Section. 1,2-Dichlorobenzene was used as solvent to maximize product yield, as C_{60} has a 10-fold higher solubility compared to toluene. The salient features of this apparatus are that (a) it allows observation of precipitation via a 3 cm-thick sapphire window, (b) the organic solution is held in a glass cradle or boat (capacity 6 mL), and (c) there is a stirrer which acts as a gentle paddle and is used after precipitation is complete to assist the mixing of the solvent with the CO_2 phase. Clearly, the fluid dynamics and surface-to-volume ratio of this system are different from those of the apparatus shown in Figure 2, but the $C_{60}(CO_2)_x$ precipitated in the two view cells was found to be identical via SEM and FT-IR microscopy. Thus, the method is inherently scalable, allowing for multigram batch production, the limiting factor being the size of pressure vessel available.

Our samples of $C_{60}(CO_2)_x$ appear to be relatively stable for FT-IR, XRD, and ^{13}C NMR analysis over a period of many days, in line with the quantitative study by Gadd et al.[6] on $C_{60}(CO_2)_x$ using thermogravimetric analysis (TGA), which showed a loss of CO_2 at room temperature from $x = 0.78$ to 0.62 over 1000 h and no further significant loss over the next 5000 h.

SEM−Examination of Crystallite Morphology

SEM of both **I** and **III** are shown in Figure 4. Sample **I**, which was rapidly precipitated via the coaxial nozzle, consists of well-distributed aggregates of very small particles, typically 200 nm (see Figure 4a,b).

Product **III**, precipitated slowly from a toluene solution, consists of particles with remarkably regular shapes derived in some cases from octahedra and in others from hexagonal plates or rods (see Figure 4c,d). With saturated toluene solutions of C_{60}, the morphology of **III** is dependent on the rate of pressurization: when the CO_2 pressure is increased slowly, significantly larger crystallites are formed of 50−100 μm (Figure 4d), compared to 10−30 μm for the faster pressurization (Figure 4c). This suggests that, in the case of toluene, the rate of crystal growth is directly related to rate of introduction of antisolvent: toluene is able to absorb large quantities of CO_2. When the solvent was not completely removed, significant damage to the particles appeared to occur after crystallization. CO_2 outgassing during depressurization is the most likely cause of the pitted and fractured octahedral crystals (see Figure 4d,f).

Characterization of $C_{60}(CO_2)_x$

IR Spectroscopy. All precipitates were studied by FT-IR microscopy, which confirmed that our precipitated samples all contained CO_2. The FT-IR microscopy spectra of **I**, **II**, and **III** were very similar. As shown in Figure 5, they display fundamental vibrational modes[13,41] for C_{60} at 1429 and 1182 cm^{-1}. A strong band at 2332 cm^{-1}, present in the spectra of all

(39) Darr, J. A.; Poliakoff, M. *Chem. Rev.* **1999**, *99*, 495−541.

(40) Vapor−liquid equilibrium curves were calculated using a modified Peng−Robinson[30] equation of state; mixture parameters were obtained by fitting experimental data from the literature. Calculations were carried out using software (SUPERTRAPP Version 2.01) supplied by NIST (National Institute of Standards and Technology, Gaithersburg, MD 20899).

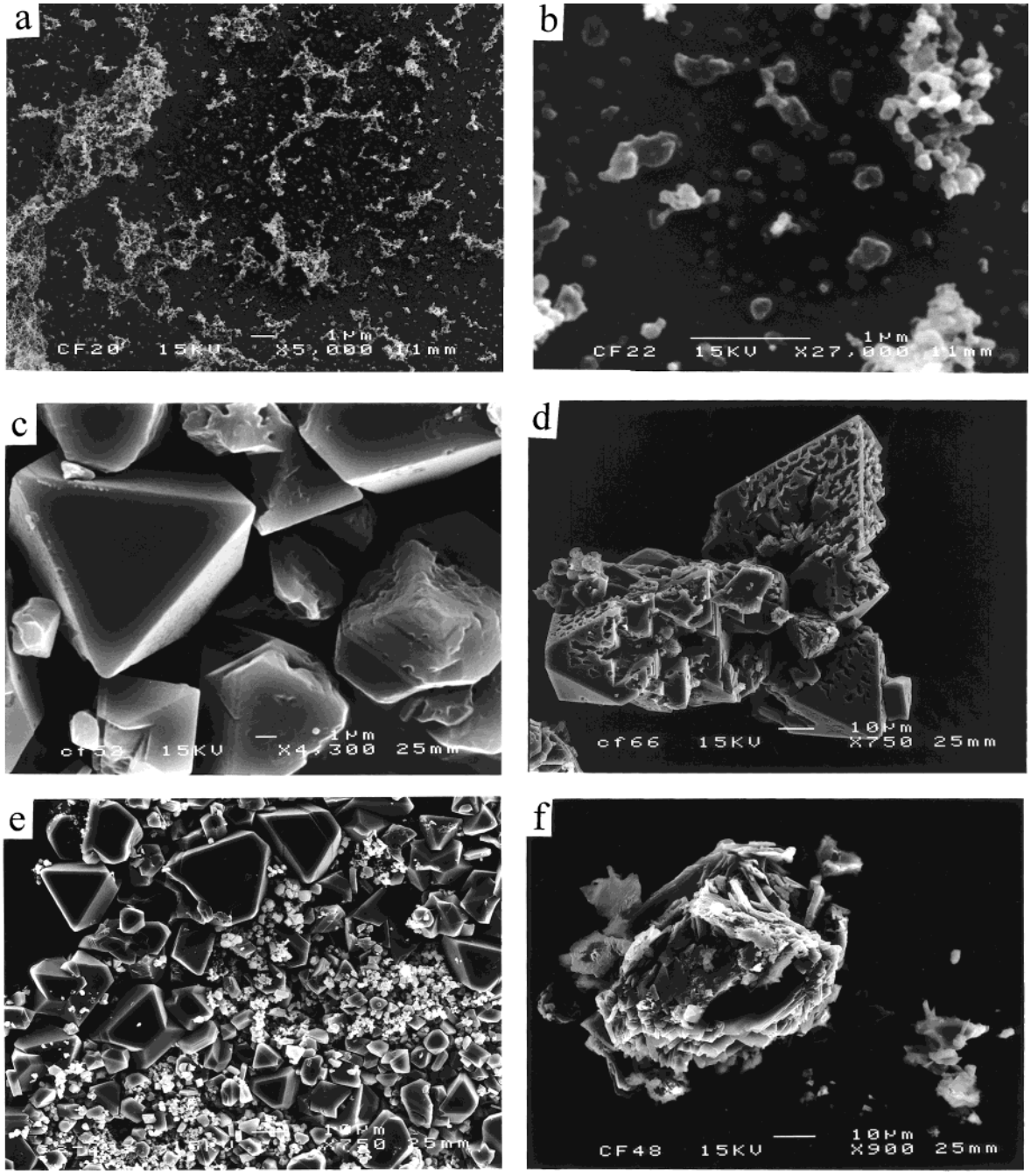

Figure 4. SEM images of $C_{60}(CO_2)_x$, where (a) and (b) show product **I** via classical PCA from toluene solution and (b) is a magnification of the central region of (a); (c) and (d) show product **III** crystallized slowly (ca. 1 bar min^{-1} antisolvent) from a toluene solution; (e) and (f) show product **III** crystallized slowly (ca. 1 bar min^{-1} antisolvent) from a 1,2-dichlorobenzene solution. In (c) the solvent, toluene, was completely removed before depressurization, while (d) shows a product in which toluene was not completely removed before depressurization; (e) shows the case in which the solvent, 1,2-dichlorobenzene, was removed before depressurization while for (f) it was not completely removed.

three products, can be assigned to the antisymmetric stretch[8] of CO_2, where the rotational fine structure has been quenched by trapping of the CO_2 or hindering of its rotation. Diffuse reflectance spectra (DRIFTS) of these samples show additional bands at 576 and 523 cm^{-1} due to the remaining fundamentals of C_{60} as well as a band at 651 cm^{-1} corresponding to the ν_1 bending mode of CO_2. The four fundamental bands for C_{60} are unshifted from those of the unprecipitated starting material. The CO_2 could either be trapped within the bulk of the C_{60} or merely be located on the surface. Chemisorbed CO_2 on the surface of C_{60} would be expected to exhibit a substantial shift in ν_3 to lower energy by >100 cm^{-1}, and possibly the IR-inactive ν_2 symmetric stretch at 1336 cm^{-1} might become IR-active. If, however, CO_2 were merely physisorbed on the surface, it would be expected to show a small perturbation in the ν_3 stretch of CO_2, such as is observed in the products **I**−**III**. However, the different particle size of products **I** and **III** means that the surface area of product **III** is ca. $\times 10^4$ smaller than that of **I**. Nevertheless, the CO_2 ν_3 IR band was of similar intensity in **I**, **II**, and **III**. Thus, the IR spectra show that CO_2 is almost certainly located in the bulk of the sample rather than on the surface.

Dissolving the brown product, **II**, in CH_2Cl_2 confirmed that CO_2 is trapped within the crystallites. The FT-IR spectrum of

(41) Taylor, R.; Hare, J. P.; Abdul-Sada, A. K.; Kroto, H. W. *J. Chem. Soc., Chem. Commun.* **1990**, 1423−1425.

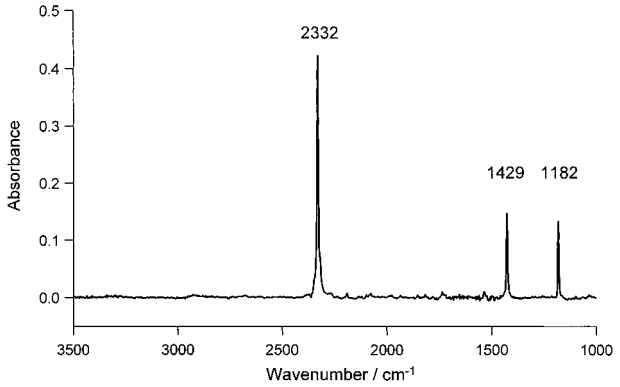

Figure 5. IR spectrum of the product $C_{60}(CO_2)_x$. The IR spectrum does not vary significantly between products **I**, **II**, and **III**. The bands at 576 and 523 cm^{-1} for C_{60} and 651 cm^{-1} for CO_2 lie below the range of the IR microscope.

the resulting solution (1 mm path length) had a band at 2338 cm^{-1} due to CO_2 released from the $C_{60}(CO_2)_x$ as well as three fundamental C_{60} bands at 1182, 576, and 525 cm^{-1}, with a fourth band expected in the region of 1429 cm^{-1} but obscured by CH_2Cl_2 absorptions. An identical band was observed at 2338 cm^{-1} when CO_2 gas was briefly bubbled through CH_2Cl_2. This experiment also eliminates the possibility that the CO_2 could be trapped inside the C_{60} ball as $CO_2@C_{60}$. This is not surprising because the van der Waals "vacuum" inside the C_{60} cage has a diameter of 3.48 Å,[42] much smaller than the van der Waals length of CO_2 of 5.36 Å.[43] Further confirmation of the bulk incorporation of CO_2 into these samples of C_{60} is provided by ^{13}C solid-state NMR (see below).

The IR bands of CO_2 were present even in the spectra of samples of **III**, which were not fully dried by CO_2. Furthermore, these spectra showed no bands of incorporated organic solvent. This suggests that CO_2 has preferentially entered the C_{60} crystal lattice *during* precipitation and has not merely displaced the solvent following precipitation.[44]

^{13}C Solid-State NMR. Carbon-13 solid-state MAS NMR spectra, recorded at room temperature, are shown in Figures 6 and 7, where (a) and (b) in each figure refer to C_{60} and **III**, respectively. In Figure 6 (4 kHz MAS rate), the most intense line in both spectra is at 143 ppm, corresponding to the isotropic chemical shift of C_{60}.[45,46] The most significant difference between the spectra is the appearance of a small signal at 124 ppm in the spectrum of product **III** (b, see inset) (see Figure 6), which is characteristic of CO_2.[47,48] Deconvolution of spectrum b with Lorentzian lines gives an intensity ratio of 0.96:60 measured via peak area for the CO_2 line relative to the total C_{60} signal (center and sidebands). This implies a CO_2 occupancy of 96%. A similar analysis of the spectrum of product **II** (not illustrated) gives a significantly reduced CO_2 occupancy of ca.

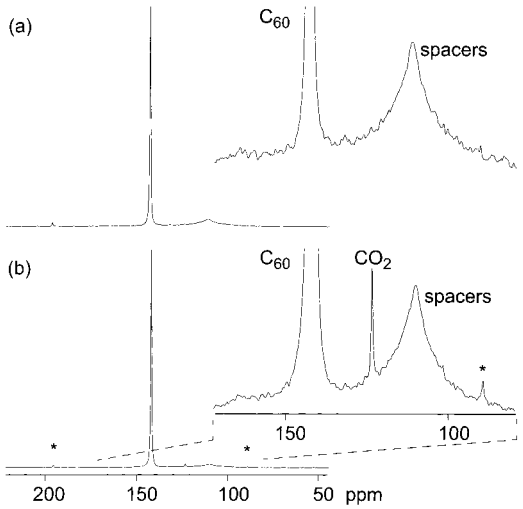

Figure 6. Solid-state carbon-13 MAS NMR spectra recorded at 293 K for (a) the starting material and (b) product **III** at spinning rates of 4 kHz. The spectra correspond to approximately 100 mg of starting material and 140 mg of product **III**, respectively. The spectra have been arbitrarily scaled so that the intensities of the C_{60} line at 143 ppm are identical. The inset shows an expansion of the region from 80 to 170 ppm. Note the appearance of a signal at 124 ppm corresponding to CO_2 in the spectrum of product **III**. The relative intensities imply a CO_2 occupancy of 96%. The small asterisked signals at 90 and 195 ppm are spinning sidebands, while the broad peak at 111 ppm arises from the fluorinated polymers used as sample spacers. No attempt has been made to subtract out this background signal.

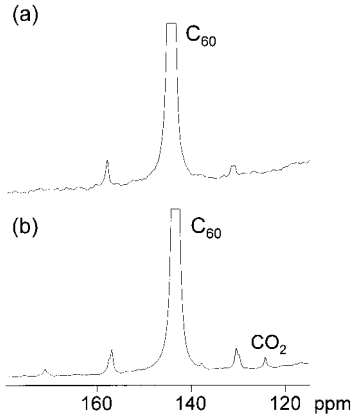

Figure 7. NMR spectra, as for Figure 6, but with a spinning rate of 1 kHz. Note the spinning sidebands which appear to be more intense and extend further in frequency for product **III** (b) compared with the starting material (a). This suggests that the C_{60} molecules tumble more anisotropically on their lattice sites in the presence of CO_2.

20%. Saturation recovery measurements result in a carbon-13 spin−lattice relaxation time T_1 of approximately 20 s for C_{60} and significantly less for CO_2, although the low signal intensity of the CO_2 line precludes a more accurate measurement.

Figure 7 shows the MAS spectra obtained at slower spinning rate, 1 kHz, with the appearance of spinning sidebands associated with the C_{60} resonance. The sidebands in the spectrum of product **III** (b) are more intense and extend further in frequency than those for the pure C_{60} (a). This suggests that, in $C_{60}(CO_2)_x$, the C_{60} molecules tumble more anisotropically on their lattice sites due to CO_2 lodged in the octahedral lattice sites. Similar conclusions about the increased anisotropy of C_{70} molecules have been drawn from the increased spinning sideband intensities[45] compared with C_{60}. In the corresponding spectrum of product **II** (not illustrated), this effect appears to be even more

(42) Taylor, R. *The Chemistry of Fullerenes*; World Scientific: Singapore, 1995.
(43) Olthof, E. H. T.; van der Avoird, A.; Wormer, P. E. S. *J. Chem. Phys.* **1996**, *104*, 832−847.
(44) FT Raman spectroscopy of the products was attempted using a relatively low laser power, 800 mW. Although the characteristic bands of C_{60} were observed, no bands were observed which could be assigned to the trapped CO_2.
(45) Tycko, R.; Haddon, R. C.; Dabbagh, G.; Glarum, S. H.; Douglass, D. C.; Mujsce, A. M. *J. Phys. Chem.* **1991**, *95*, 518−520.
(46) Yannoni, C. S.; Johnston, R. D.; Meijer, G.; Bethune, D. S.; Salem, J. R. *J. Phys. Chem.* **1991**, *95*, 9−10.
(47) Beeler, A. J.; Orendt, A. M.; Grant, D. M.; Cutts, P. W.; Michl, J.; Zilm, K. W.; Downing, J. W.; Facelli, J. C.; Schindler, M. S.; Kutzelnigg, W. *J. Am. Chem. Soc.* **1984**, *106*, 7672−7676.
(48) Hwang, S.-J.; Petucci, C.; Raftery, D. *J. Am. Chem. Soc.* **1998**, *120*, 4388−4397.

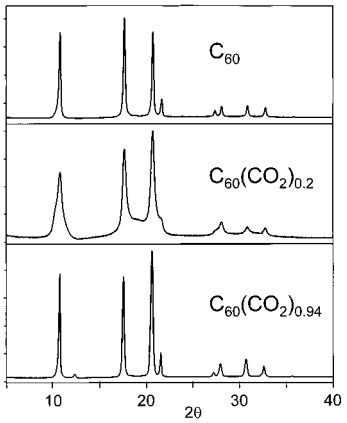

Figure 8. Powder XRD of the starting material C_{60} (upper), product **II** $C_{60}(CO_2)_{0.2}$ (middle), and product **III** $C_{60}(CO_2)_{0.94}$ (lower).

pronounced, possibly because of more unequal occupancy of CO_2 about a given C_{60} molecule.

Powder XRD. Figure 8 compares the powder X-ray diffractograms of the starting material (C_{60}) with those of **II** and **III**. The diffractogram of C_{60} before precipitation is generally in line with published data[49,50] for C_{60}. The broadness of the reflections in the diffractogram of the product **II** indicates that the crystallite size was, indeed, much smaller than that of the starting material, in agreement with the SEM images of product **I** produced during the same experiment (see Figure 4a,b). This contrasts with the sharpness of the lines in the XRD of the more crystalline **III**, which is consistent with that reported by Gadd et al.[6] for $C_{60}(CO_2)_x$, both in the anomalous intensities of the stronger reflections and also in the appearance of minor extra reflections. Thus, the crystal structures of our material and theirs are almost certainly the same, i.e., a face-centered cubic (fcc) lattice at room temperature with CO_2 occupying the octahedral interstitial sites.

There are well-documented difficulties in obtaining a reliable refined structure of C_{60} and its derivatives at room temperature by X-ray diffraction.[51] Apart from the inherent problems of locating light elements, a quantitatively meaningful model is often precluded by a combination of static disorder and stacking fault effects. Nevertheless, approximations can be made to obtain chemically useful information from room temperature data. A spherical shell approach has been successfully employed for fullerenes, modeling each C_{60} molecule as a sphere of electron density of radius ca. 3.5 Å using a zero-order Bessel function.[52,53] Electron diffraction has also been used to map regular icosahedra of C atoms with average rotational disorder and fit these to coordinates in space groups *Fm*3*m* or *Fm*3.[54] Atomic positions of the C framework from these models of C_{60} and its intercalates[6,55] at room temperature were taken as our initial

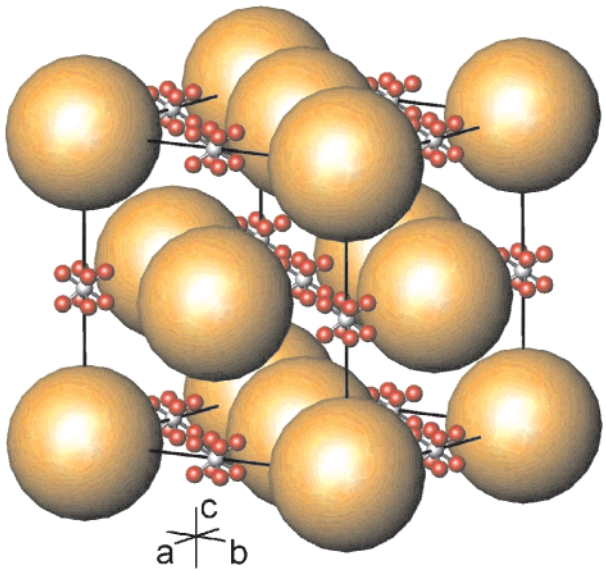

Figure 9. Simplified representation of the structure of $C_{60}(CO_2)_x$. The C_{60} molecules are represented by a spherical shell of electron density of approximate radius 3.5 Å. CO_2 molecules partially occupy the octahedral interstitial sites of the fcc unit cell with the O atoms disordered over the *32*f positions. (*R* factors: $R_I = 11.67\%$, $R_p = 10.33\%$, $R_{wp} = 15.93\%$, $R_e = 0.33\%$; for full details of the refinement see Results and Discussion.)

structural basis. In our starting model, CO_2 molecules were placed within the octahedral interstices of the *Fm*3*m* cubic, room-temperature structure of C_{60}, as described by Gadd et al.[6,7] C was therefore positioned on the ($^1/_2$,$^1/_2$,$^1/_2$) site and O disordered across the *32*f (*x*,*x*,*x*) sites with $x = 0.452$. At the outset of the refinement, temperature factors were fixed at 6 Å^2 for C_{60} C atoms and at unity for the CO_2 C and O atoms. Occupancy factors were set to 100% for all C atoms. The crystallographic occupancy of O was fixed as twice that of C in the CO_2 molecules.

The validity of the starting model was tested using POWDERCELL 2.0[56] to generate a theoretical powder pattern based on the crystallographic parameters taken from models of C_{60} and $C_{60}(CO_2)_x$. This theoretical pattern was in good agreement with the collected data. Importantly, removal of CO_2 from the model structure made significant differences in the relative intensities of the lower angle reflections (e.g., 111, 220, 311, etc.) and led to the complete disappearance of the 200 peak. A simplified model of the $C_{60}(CO_2)_x$ structure, representing each C_{60} as a spherical shell of electron density of radius ~3.5 Å, is shown in Figure 9.

Early stages of the refinement concentrated on varying scale factor, zero-point, lattice parameters, and profile parameters while leaving atomic parameters unchanged. Refinements were attempted utilizing either interpolated background or a polynomially fitted background, but the latter option led to recurrent instability. Peak shapes were fitted to the pseudo-Voigt function. It has been previously noted that [111] stacking fault defects are problematic in peak fitting, particularly at low 2θ values.[6,54] Similar problems were encountered in refinement of **III**, and these were minimized, but not removed, by careful and gradual refinement of half-widths, mixing parameters, and the asymmetry function. Alternative peak shape functions did not improve the fit, and no attempt was made to exclude peak shoulders from the refinement lest crystallographic information be inadvertently lost.

(49) Luzzi, D. E.; Fischer, J. E.; Wang, X. Q.; Ricketts-Foot, D. A.; McGhie, A. R.; Romanow, W. J. *J. Mater. Res.* **1992**, *7*, 335−340.
(50) Werner, H.; Bublak, D.; Göbel, U.; Henschke, B.; Bensch, W.; Schlögl, R. *Angew. Chem., Int. Ed. Engl.* **1992**, *31*, 868−870.
(51) Fleming, R. M.; Seigrist, T.; Marsh, P. M.; Hessen, B.; Kortan, A. R.; Murphy, D. W.; Haddon, R. C.; Tycko, R.; Dabbagh, G.; Mujsce, A. M.; Kaplan, M. L.; Zahurak, S. M. *Mater. Res. Soc. Symp. Proc.* **1991**, *206*, 691.
(52) André, D.; Dworkin, A.; Szwarc, H.; Céolin, R.; Agafonov, V.; Fabre, C.; Rassat, A.; Straver, L.; Bernier, P.; Zahab, A. *Mol. Phys.* **1992**, *76*, 1311−1317.
(53) Chow, P. C.; Jiang, X.; Reiter, G.; Wochner, P.; Moss, S. C.; Axe, J. D.; Hanson, J. C.; McMullen, R. K.; Meng, R. L.; Chu, C. W. *Phys. Rev. Lett.* **1992**, *69*, 2943.
(54) Dorset, D. L.; McCourt, M. P. *Acta Crystallogr. A* **1994**, *50*, 344.
(55) Gadd, G. E.; Elcombe, M. M.; Dennis, J.; Moricca, S.; Webb, N.; Cassidy, D.; Evans, P. J. *J. Phys. Chem. Solids* **1998**, *59*, 937−944.
(56) Nolze, G.; Kraus, W. *Powder Diffract.* **1998**, *13*, 256.

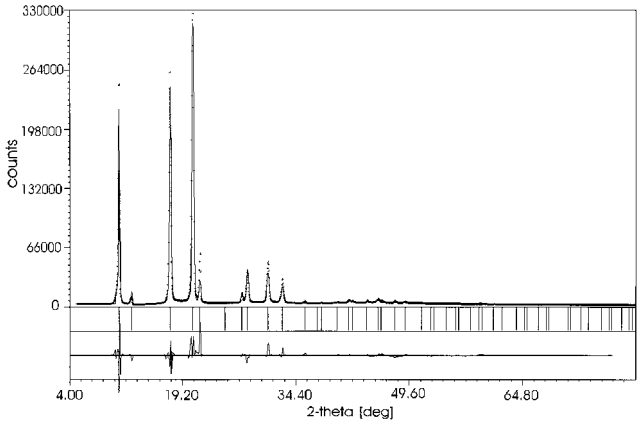

Figure 10. Observed (crosses), calculated (upper solid line), and difference (lower solid line) (OCD) profiles for the refinement of $C_{60}(CO_2)_{0.94}$. Allowed reflections are indicated by tic marks.

Table 1. Final Positional and Thermal Parameters for $C_{60}(CO_2)_{0.94}$ (Space Group $Fm3m$; $a = 14.240(1)$ Å)

atom	*x*	*y*	*z*	B/Å$^{2\,a}$
C1[b]	0.053	0	0.255	9.3(3)
C2[b]	0.107	0.084	0.219	9.3(3)
C3[b]	0.182	0.053	0.150	9.3(3)
C[c]	0.5	0.5	0.5	4.1(22)
O[c]	0.451(1)	0.451(1)	0.451(1)	4.1(22)

[a] Where $B = {}^4/_3[a^2B_{11} + b^2B_{22} + c^2B_{33} + ab(\cos\gamma)B_{12} + ac(\cos\beta)B_{13} + bc(\cos\alpha)B_{23}]$. For the space group $Fm3m$ (No. 225), this simplifies to $B = {}^4/_3[a^2\beta_{11} = b^2\beta_{22} = c^2\beta_{33}]$. [b] Final site occupancy fixed at 72%, 71%, and 77% for C1, C2, and C3, respectively. [c] Final occupancy of CO_2 fixed at 94%.

Intermediate stages of the refinement concerned the location and disorder of the C_{60} framework. C positions were varied atom by atom, maintaining the stability of the refinement. Isotropic temperature factors were gradually introduced, although the B values were constrained to the same value and varied. A further approximation of static and dynamic disorder was introduced by varying C site occupancies. This approach was found to be notably more successful than varying C_{60} and CO_2 *positional* parameters simultaneously later in the refinement, which despite leading to lower R factors also induced extreme levels of distortion in the C_{60} framework and destabilized the refinement. Occupancies and temperature factors were varied alternately until convergence was reached to avoid correlations. "Final" positions, temperature factors, and occupancies at this stage reflect a strongly disordered C_{60} environment, perhaps indicative of the heightened anisotropic tumbling observed from the ^{13}C MAS NMR data.

The CO_2 environment was examined in the final stages of the refinement. C_{60} atomic positions remained fixed in these final stages as noted above. The C atom site occupancy was left to vary independently while temperature factors and the O position and occupancy were fixed. This refined to a 94% occupation, which agreed very closely with the ^{13}C MAS NMR data. It was subsequently fixed with the *crystallographic* O occupancy set at twice this level. The positional parameters of O and the C and O isotropic temperature factors (which were tied) were then varied, initially independent of the C_{60} framework variables and then in final cycles, concurrently. Final R factors for the refinement were $R_I = 11.67\%$, $R_p = 10.33\%$, $R_{wp} = 15.93\%$, and $R_e = 0.33\%$. The observed, calculated, and difference profiles for $C_{60}(CO_2)_{0.94}$ are shown in Figure 10, and the final positional and thermal parameters are shown in Table 1.

Although, perhaps, this model for **III** can be viewed as semiquantitative at best, the final fit is remarkably consistent with other reported structures of fullerenes and intercalates.[6,7,52,54] The occupancy level from our best-fit model, 0.94, is very close to that derived from ^{13}C NMR data (0.96). Furthermore, the resulting structural modifications correlate well with the previously reported $C_{60}(CO_2)_x$ compounds[6,7] with lower levels of intercalated CO_2. It is interesting to note, however, that the refined C═O bond length (1.20(3) Å) is significantly closer to that in the free molecule[57] (1.165 Å) than has previously been reported[6] (1.29(1) Å).

We have calculated the lattice parameters for each sample. For the starting material, 14.169(1) Å compares well with a room-temperature lattice parameter of 14.152 Å found for pure C_{60} through single-crystal work[49,52] and 14.17 Å found through powder XRD work.[58] Sample **III**, $C_{60}(CO_2)_{0.95}$, 14.243(3) Å, is close to the value, 14.224 Å, reported for $C_{60}(CO_2)_{0.8}$.[7] Sample **II**, $C_{60}(CO_2)_{0.2}$, has an intermediate value, 14.182(5) Å, showing that the lattice expands progressively as the CO_2 occupancy increases.

The interaction between CO_2 and C_{60} molecules in $C_{60}(CO_2)_x$ appears to be a fine balance between electrostatic and van der Waals contributions, which become more anisotropic at low temperature.[7] It would seem likely that as CO_2 intercalation levels increase, C_{60} molecules are forced farther apart isotropically at room temperature. Neutron diffraction studies will be needed before a more detailed explanation can be given of the progressive effect of increased doping levels on structure and bonding at room temperature and below.

Conclusions

We have described two different strategies for precipitating C_{60} from saturated organic solutions using compressed CO_2 as the antisolvent. The products have been shown to contain large amounts of CO_2, and our results and analysis strongly suggest that CO_2 is lodged in the octahedral sites of the C_{60} lattice, giving an intercalate $C_{60}(CO_2)_x$, where $x = 0.2$ for the submicron material precipitated rapidly and $x = 0.95$ for the larger crystallites precipitated more slowly. The CO_2 enters the C_{60} crystal lattice during crystal growth and has not simply exchanged with cocrystallized organic solvent during the drying step, as shown by the presence of CO_2, the absence of organic solvent, and the intrinsic crystallinity of the products formed by slow crystallization.

As with the development of many new materials, the discovery[8] and the subsequent characterization and improved synthesis[6,7] of $C_{60}(CO_2)_x$ initially involved very specialized experimental conditions. Now we have described an alternative strategy which is, we believe, more accessible to the synthetic chemist and provides two very different routes toward $C_{60}(CO_2)_x$, giving either submicron, relatively amorphous material where CO_2 occupancy is low or microcrystalline $C_{60}(CO_2)_x$ where the CO_2 level is high. There are several points regarding our studies on $C_{60}(CO_2)_x$ which need stressing. First, this precipitation method avoids the high temperatures, the very high pressures, and the long times currently used in other routes[6,8] to $C_{60}(CO_2)_x$, yet the CO_2 content obtained by our route is higher. The precipitation is fast: precipitation occurs either on approximately a millisecond time scale in the case of the

(57) Herzberg, G. *Molecular Spectra and Molecular Structure, II Infrared and Raman Spectra of Polyatomic Molecules*; Van Nostrand Reinhold: New York, 1945; Vol. II.

(58) Heiney, P. A.; Fischer, J. E.; McGhie, A. R.; Romanow, W. J.; Denenstein, A. M.; J. P. McCauley, J.; A. B. Smith, I.; Cox, D. E. *Phys. Rev. Lett.* **1991**, *66*, 2911−2914.

submicron material, or over hour(s) in the case of the more crystalline material. This more crystalline material, $C_{60}(CO_2)_{0.95}$, has been produced on a relatively large scale, 140 mg per batch, and there is no reason this approach cannot be scaled up further. Second, $C_{60}(CO_2)_x$ has been produced directly from an organic solution and was found to be completely solvent-free upon precipitation. In fact, the amount of solvent extracted with CO_2 using the two methods described in this paper is the same as or less than that which would be used to separate C_{60} on a column prior to recrystallization in preparation for the synthesis of $C_{60}(CO_2)_x$ by previously published routes. Furthermore, the morphology can be controlled by both the method of solution introduction in the case of yellow-brown submicron crystalline powders, and the rate of pressurization in the case of the highly crystalline material formed during the layering experiment. Our approach should be applicable to the production of many other coprecipitated or encapsulated fullerene products.

Acknowledgment. We thank Jie Ke for phase behavior calculations, S. J. Barlow for the solution FT-IR, P. B. Webb for the FT-IR microscopy, K. Stanley for technical assistance, and Professor M. A. Chesters and Dr. M. G. Barker for helpful discussions. We thank the EPSRC for Research Grant No. GR/L26742 (J.J.T.) and ROPA Grant No. GR/L70950 (M.P.). D.H.G. thanks the EPSRC for an Advanced Fellowship, and M.P. thanks the Royal Academy of Engineering for a Clean Technology Fellowship.

JA9919478